Numerical Simulations of Rarefied Gas Flows in Micronozzles

Shashank Jaiswal · **Nishanth Dongari** (✉) · **Vijay Kumar Saraswat**
Department of Mechanical & Aerospace Engineering
Indian Institute of Technology Hyderabad
email: nishanth@iith.ac.in

Submitted to :

Submitted :

Abstract

The present study is concerned with the modelling of slip regime flow behavior in micronozzles using both the DSMC and Knudsen-layer models. We carry out our numerical simulations using open-source Computational Fluid Dynamics (CFD) and Direct simulation Monte-Carlo (DSMC) solvers available in OpenFOAM. The Navier-Stokes-Fourier (N-S-F) constitutive relations and non-equilibrium boundary conditions have been extended to capture the non-linear flow behavior associated with the Knudsen layer. In our study, the Knudsen number ranges from $0.005 \leq \mathrm{Kn} \leq 0.05$, and the associated throat Reynolds number varies from 5 to 500. For a given Knudsen number, DSMC and Knudsen layer results predict higher specific impulse compared to the conventional N-S-F model due to the shear thinning effect in the near-wall region. Owing to the inherent low Reynolds number of the flow, substantial viscous subsonic layers develop at the boundaries of the micronozzle, and their thickness is governed by Knudsen number. The viscous subsonic layer retards the bulk flow, and results in a decrease in nozzle thrust, and hence it is pertinent to predict the layer thickness accurately. The distribution of various flow parameters such as pressure, Mach number, slip velocity, and wall shear stress have been also reported. The simulation results indicate that the classical N-S-F equations along with the slip and jump boundary conditions, strongly deviate from DSMC. On the other hand, Knudsen-layer model shows fair agreement with the DSMC data, thereby improving the predictive capabilities of conventional N-S-F relations.

Keywords : Micronozzles, Viscous Layer, Rarefied Gas flows, OpenFOAM, DSMC

Nomenclature

Kn	Knudsen Number
Pr	Prandtl Number
p	Pressure (Pa)
U	Velocity (m/s)
T	Temperature (K)
Ma	Mach number
H	Characteristic length scale
d	Molecular diameter (m)
δ	Mean molecular separation (m)
m	Molecular mass (kg)
tr	trace
I	Identity tensor
S	Transformation tensor
v	Boundary patch normal
R	Specific gas constant
A_s	First Sutherland coefficient (kg/(s.m.K$^{1/2}$))
T_s	Second Sutherland coefficient (K)
∇	Gradient
∇_{n}	Gradient normal to boundary patch
γ	Specific heat ratio
λ	Unconfined gas mean free path
λ_{eff}	Effective gas mean free path
β_{PL}	Normalized effective mean free path for momentum transfer
$(\beta_{\mathrm{PL}})_{\mathrm{T}}$	Normalized effective mean free path for energy transfer
ρ	Density (kg/m^3)
μ	Dynamic viscosity (kg/ms)
μ_{eff}	Effective dynamic viscosity (kg/ms)
ψ	Compressibility (s^2/m^2)
κ	Thermal conductivity (W/mK)
κ_{eff}	Effective thermal conductivity (W/mK)
Π_{mc}	Curvature Effect
σ_v	Momentum accommodation coefficient
σ_t	Thermal accommodation coefficient

Superscripts / Subscripts

w	wall
th	throat
ex	exit
i	inlet
o	outlet
T	transpose
∞	freestream condition

1. Introduction

With the advent of micro-fabrication and 3-D printing methods, small scale satellites have now become cost-effective solutions to ever increasing satellite demands. Micro satellites are readily employed to carry out studies in numerous fields such as weather forecasting, communication, geographical studies and space observations. However, miniaturized satellites usually require efficient micro-propulsion, attitude control, communication and computation systems. Micro-nozzles are integral components of these miniaturized systems which are used to produce the required thrust which helps in propelling and maneuvering the satellite.

The flow behavior in micronozzles is of fundamental importance as it governs the amount of thrust generated. In microscale gas flows, the surface to volume ratio rapidly increases with a decrease in characteristic length scale, and hence the surface forces becomes dominant [1, 2]. When the characteristic length is on the order of mean free path (MFP), the gas molecule wall-surface interactions lead to the formation of Knudsen layer (KL): a local thermodynamically non-equilibrium region extending $\sim O(\lambda)$ from the surface, where λ is the gas mean free path (MFP) [3]. Here, the Knudsen number (Kn) is defined as λ/H, where H is the characteristic length. The degree of rarefaction i.e Kn affects the amount of thrust generated by the micronozzle system.

The investigation of flow behavior in nozzles date back to as early as 1964 [4], where the author emphasizes on the flow transition from continuum to free-molecular inside nozzles. Rothe et al. [5] investigated the supersonic viscous nozzle flow using electron-beam techniques, and reports the flow

density and rotational temperature at selected points in the nozzle. An agreement between experimental and numerical investigations by Boyd et al. [6] established that direct simulation Monte-Carlo (DSMC) could provide an accurate description of flow in micronozzles. Hao et al. [7] measured the mass flow rates and pressure distributions near the nozzles throat under various outlet pressures experimentally. Xie et al. [2] carried out DSMC and N-S-F simulations, and reported the characteristics of gas flows for different micronozzle geometric configurations. Xu et al. [8] analyzed oblique shock structures in micronozzles using Navier-Stokes equations with slip boundary conditions. San et al. [9] analyzed the effect of variation of size and expansion ratio. Saadati et al. [10] carried out DSMC simulation on nanonozzle flows. While the experiments have repeatedly focused on measurement of bulk properties which may not be indicative of the dynamics of the entire micronozzle flow, the DSMC or Kinetic theory based simulations are too computationally intensive.

In case of a linear converging-diverging (C/D) type micronozzle, the flow experiences the continuum behavior as well as the rarefied condition, and hence the Knudsen number varies from continuum to early transition regimes. Ideally, DSMC simulations [11–14] provide accurate predictions in the KL region of micronozzles. However, the DSMC method is computationally intensive for low-speed flows in the slip regime, and large scale 3-D complex geometries. The conventional Navier-Stokes-Fourier (N-S-F) relations along with slip/jump boundary conditions fail to accurately capture the non-linear flow behavior observed in the Knudsen layer [3,15–17]. Alternatively, Knudsen layer based [15,18–25] modelling techniques have been incorporated to extend the applicability of the N-S-F equations in the near wall region. Guo et al. [18] suggests an extension of N-S-F equations to larger Kn by incorporating the gas molecular interactions with the boundary walls through modification of the classical expression of the MFP. Using a similar approach, Arlemark et al. [22] captured Poiseuille velocity flow profiles and the Poiseuille mass flow rate in planar geometries. Guo et al. [24] captured several effects observed in micro-channel gas flows using extended N-S-F and a second order slip boundary condition.

Dongari et al. [21,26] hypothesized that the probability distribution function for the MFP of a rarefied gas followed a PL form, which was validated against MD data under various rarefied conditions. Using a PL distribution to describe free paths, the authors [21,23,27,28] derived effective MFP models

for flows confined by planar and non-planar surfaces, by taking into account the solid boundary effects. The authors [23, 27, 28] modified the constitutive N-S-F relations and slip boundary conditions using power-law based effective MFP modelling, which scales the transport properties, resulting in non-linear viscosity and thermal conductivity. The MFP based scaling captured several non-equilibrium effects in the Knudsen layer. While the classical exponential MFP scaling approaches [19, 22] are limited up to Kn $\sim$ 0.2, power-law based effective MFP models exhibit good agreement up to the early transition regime (Kn $\sim$ 1) [24]. The MFP based scaling has been incorporated in Lattice-Boltzmann models as well. [29]. Recently, Jaiswal et al. [30] captured various Knudsen layer effects associated with low and high-speed rarefied gas flows in slip and transition regimes using an effective MFP modelling for planar geometries.

Hence, in the current paper, we have investigated the flow behavior in micronozzles using the DSMC method, and the results compared against the conventional slip/jump and Knudsen-layer based CFD models. An open-source *dsmcFOAM* [12,31] solver has been used for carrying out DSMC simulations. We have implemented the PL-based MFP model in an open source CFD package OpenFOAM®. The PL-based MFP scaling is incorporated in a density-based compressible solver *rhoCentralFoam* [32] by creating a new set of thermo-physical properties modelling routines, and the velocity slip and temperature jump boundary conditions. Our *knudsen layer model* results are compared against DSMC data. A total of five test cases, covering the slip flow regime, have been simulated. We report the pressure and velocity flow profiles, as well as specific impulse along with shear stress at walls.

2. Numerical Simulations

OpenFOAM [33, 34] (Open Field Operation and Manipulation) CFD Toolbox is a free, open source CFD software package which has an extensive range of features to solve complex fluid flow problems for arbitrary structured and unstructured grids. Using C++ [35] as it's base language, and the concepts of OOP and templating [33], OpenFOAM provides an excellent framework for incorporation & implementation of novel flow computation models. Various solvers (for example: *dsmcFOAM* [12], *rhoCentralFOAM* [32], etc) present in OpenFOAM has been a direct result of contribution from the sci-

entific community. The primary solvers (including meshing, and pre-processing and post-processing) run in parallel using the method of domain decomposition and Massage Passing Interface (MPI) between processes on host, enabling the users to take full advantage of host computer.

2.1. rhoCentralFOAM

A second order accurate central scheme (in terms of numerical viscosity $\sim$O($\triangle x^{2r-1}$)) has been recently proposed by Kurganov and Tadmor [36], and consequently the authors proposed the semi-discrete central scheme formulation [37] as the second order generalization of the celebrated Lax-Friedrichs scheme [32, 36] for hyperbolic conservation laws. *rhoCentralFOAM* [32] is a density based compressible solver available in OpenFOAM, which implements the semi-discrete central scheme formulation as proposed by Kurganov and Tadmor [37]. The original solver models & implements the conventional compressible Navier-Stokes and Internal Energy along with the continuity equation (See [32]). The solver is a coupled implicit smooth solver with standard Gauss-Seidel as smoother. The time derivatives are discretized using the standard implicit Euler scheme. The interpolation procedure is split into two directions corresponding to flow outward and inward of the cell. And, the two directions are weighted equally for the purpose of calculation of gradient and convective terms, hence its description as central scheme. The solver has the capability to simulate arbitrary 2D/3D geometries with a variety of boundary conditions (Dirichlet, Neumann or Robin), and has been benchmarked [32] & widely used for studying hypersonic [38], subsonic [39] and thermal [40, 41] gas flow problems.

2.2. dsmcFOAM

The direct simulation Monte Carlo (DSMC) method [11], based on the kinetic theory of dilute gases ($d \ll \delta$), has been increasingly used in numerical simulations at micro scales. Gas flows in micronozzles are characteristically low speed and often driven by a pressure gradient. The velocity profiles at inlet and outlet are generally not known at microscale due to experimental limitations. Liou et. al [42, 43] proposed an implicit pressure boundary condition for low speed microchannel flows. At inlet, the stream-wise mean velocity profile is derived from the first order extrapolation and time average of the stream-wise velocity profile from the boundary cells. At outlet, the pressure and density values are used to derive the velocity profile by following characteristics-theory based equations [42, 43]. The

implementation details of the same can be found in White et al. [31,44].

dsmcFOAM [12], developed at University of Strathclyde, is a discrete particle-based solver available in OpenFOAM. It employs the DSMC method as proposed by Bird [11]. The solver takes into account the rotational kinetic energy associated with the molecular rotational velocity and its moment of inertia, in addition to the translational kinetic energy. The solver has been benchmarked [12] and widely used for studying hypersonic, supersonic and thermal [10,31,44] gas flow problems.

3. Effective Transport Properties

3.1. Theoretical Development

Wall-distance scaling functions for the constitutive relationships for shear stress and heat flux have been already proposed: Kn-dependent functions [45], and power-law scaling of constitutive relations [22, 23, 46–48] to extend the validity of hydrodynamic models to the transitional regime gas flows. The method has been since then applied to study various flow effects (such as Velocity Inversion in Cylindrical Couette flows [27,28]) in non-planar geometries as well. The method proposed by Dongari et al. [21,23], valid for larger Knudsen numbers, is briefly described in the following paragraphs.

For viscous flows, the shear stress term in conventional N-S-F can be expressed as

$$\tau = -\mu\left[\nabla \mathrm{U} + \nabla \mathrm{U}^{\mathrm{tr}}\right] + \left(\frac{2}{3}\mu - k\right)(\nabla.\mathrm{U})I \tag{1}$$

where μ is the fluid dynamic viscosity, k the bulk viscosity, I the identity tensor, and tr the transpose operator.

The volume dilation effects for rarefied gases [49] can be neglected, and the dynamic viscosity can be substituted by the effective viscosity (See [21, 23, 26–28]), which yeilds a non-linear stress/strain relation:

$$\tau = -\underbrace{\mu\beta_{PL}}_{\mu_{\mathrm{eff}}(\mathrm{PL})}\left[\nabla \mathrm{U} + \nabla \mathrm{U}^{\mathrm{tr}}\right] \tag{2}$$

where β_{PL} is the normalized effective mean free path for momentum transfer (See Eq.(3.20) for planar, and Eq.(3.31, 3.35, 3.37, 3.41) for non-planar geometries in Ref. [26]).

The conventional heat flux in the energy equation can be given by:

$$q = -\kappa \nabla T \tag{3}$$

where κ is the fluid thermal conductivity, T the temperature, and q the heat flux.

Using the non-dimensional effective MFP for thermal cases, $(\beta_{PL})_{\mathrm{T}}$, a non-linear constitutive relation for heat flux, can be given by:

$$q = -\underbrace{\kappa (\beta_{PL})_{\mathrm{T}}}_{\kappa_{\mathrm{eff}}(\mathrm{PL})} \nabla T \tag{4}$$

Hence, the effective transport properties acquires the following form:

$$\mu_{\mathrm{eff}} = \mu \beta_{PL} \tag{5}$$

$$\kappa_{\mathrm{eff}} = \kappa \, (\beta_{PL})_{\mathrm{T}} \tag{6}$$

3.2. Solution Procedure: β_{PL} / $(\beta_{\mathrm{PL}})_{\mathrm{T}}$ calculation

The structured grids (as shown in Fig. 1) have been used for simulating micronozzles as evident from present literature [2, 10]. On such a grid, the effective MFP based scaling can be described as follows.

Divide the entire mesh into set of rectangular cells. If we were to draw a line perpendicular to the flow axis (say $X = L_1$), the line would pass through a set of cells which have same X coordinate but different Y coordinates. We will also find two zero-volume cells on the boundary (boundary cells) which has the same X coordinate as described by the equation of the perpendicular line. In the limiting case of infinite number of cells, the two boundary cells will be parallel to each other. For such a set of

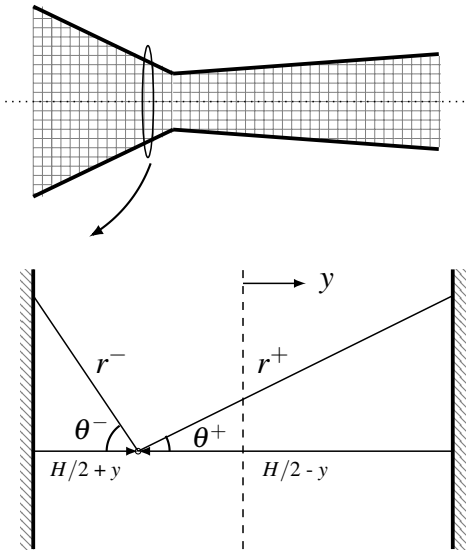

FIGURE 1: At each cross section of the micronozzle i.e series of cells in the cross-flow direction, can be treated together as series of molecules confined between two parallel walls.

two parallel walls, we can apply the power law based MFP wall scaling [23]. So, the function β_{PL} & $(\beta_{PL})_T$ has to be computed at each cross section.

But, the finite volume method considers a finite number of cells in the mesh domain. Since μ is a scalar field defined on cell-centers of collocated mesh, the correction i.e. β_{PL} / $(\beta_{\mathrm{PL}})_{\mathrm{T}}$ is also defined as a scalar field on cell-centers of collocated mesh. For the purpose of calculating β_{PL} / $(\beta_{\mathrm{PL}})_{\mathrm{T}}$, let us take a cell in internal field (A). If we travel along y axis, we will get two zero-volume cells on boundaries which will have the same x coordinate of cell-center as the chosen cell (A) in internal field. Therefore, we can calculate the distance between two patches and that will give us H. The distance from chosen cell to the boundary patches will give us r^+ and r^- respectively. The obtained values can be substituted (See Eq.(3.20) in Ref. [26]) to obtain β_{PL}. $(\beta_{\mathrm{PL}})_{\mathrm{T}}$ can also be computed similarly. A contour of β_{PL} variation inside the micronozzle has been shown in Fig.2

An important assumption that we make is that the diverging and converging angles of micronozzle is small, and the geometric mesh consists of sufficient number of cells, so that we can approximate the two patches on the boundary to be parallel to each other.

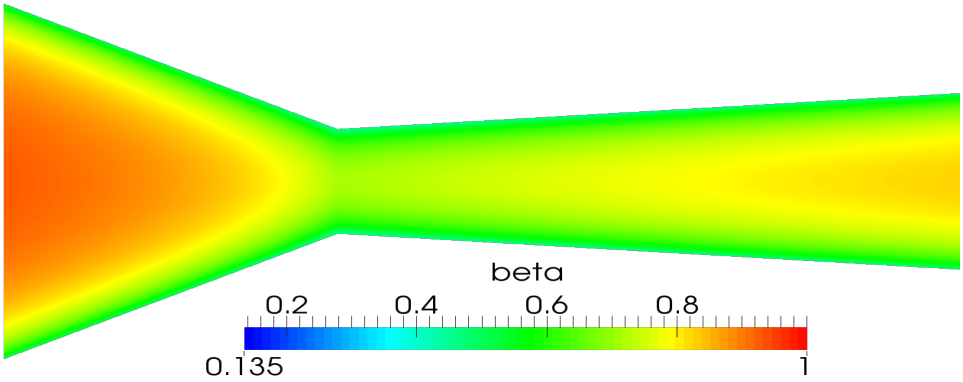

FIGURE 2: Variation of β_{PL} inside the micronozzle

3.3. Boundary Conditions

The modified N-S-F constitutive relation also needs to be solved in conjunction with the appropriate slip boundary conditions to capture the non-equilibrium phenomena in the KL [23]. OpenFOAM implements the Maxwell velocity slip and Smoluchowski temperature jump boundary conditions in the *rhoCentralFoam* solver [32]. The current implementation of Maxwell velocity slip and Smoluchowski temperature jump in OpenFOAM can be mathematically expressed as [32, 40, 50]:

$$\mathrm{U} = \mathrm{U}_w - \frac{2-\sigma_v}{\sigma_v}\lambda\nabla_n(S.\mathrm{U}) - \frac{2-\sigma_v}{\sigma_v}\frac{\lambda}{\mu}S.(v.\Pi_{mc}) - \frac{3}{4}\frac{\mu}{\rho}\frac{S.\nabla T}{T} \tag{7}$$

$$T = T_w - \frac{2-\sigma_t}{\sigma_t}\frac{2\gamma}{(\gamma+1)Pr}\lambda(v.\nabla T) \tag{8}$$

respectively, with,

$$\frac{\lambda}{\mu} = \sqrt{\frac{\pi\psi}{2}}\frac{1}{\rho} \tag{9}$$

$$\Pi_{mc} = \mu(\nabla\mathrm{U})^T - (2/3)Itr(\nabla\mathrm{U}) \tag{10}$$

where σ_v is the tangential momentum accommodation coefficient, σ_t is the thermal accommodation coefficient, U_w is wall velocity, T_w is wall temperature, v is the boundary patch normal, Pr is Prandtl number, γ is adiabatic index, and $S = I\text{-}v*v$ is the identity tensor which removes normal components of any non-scalar field, eg. velocity, so that slip occurs in the direction tangential to surface. Four terms

that appear on right side of Eq. (7) correspond to wall velocity, effects of viscous stresses, it's curvature effect and thermal creep, respectively.

For the power law based MFP modelling, using Eqs. (5) and (6), the modified velocity slip boundary condition can be expressed as :

$$\begin{aligned} \mathrm{U} = \mathrm{U}_w - \frac{2-\sigma_v}{\sigma_v}\sqrt{\frac{\pi\psi}{2}}\frac{\mu\beta_{\mathrm{PL}}}{\rho}\nabla_n(S.\mathrm{U}) \\ -\frac{2-\sigma_v}{\sigma_v}\sqrt{\frac{\pi\psi}{2}}S.(v.\Pi_{mc,\mu_{\mathrm{eff}}}) - \frac{3}{4}\frac{\mu\ (\beta_{\mathrm{PL}})_{\mathrm{T}}}{\rho}\frac{S.\nabla T}{T} \end{aligned} \tag{11}$$

In similar manner, using Eqs. (8) and (9), the Smolouchowski temperature jump boundary condition for planar geometries can be expressed as:

$$T = T_w - \frac{2-\sigma_t}{\sigma_t}\frac{2\gamma}{(\gamma+1)Pr}\sqrt{\frac{\pi\psi}{2}}\frac{\mu}{\rho}(v.\nabla T) \tag{12}$$

Using Eq. (6), the modified temperature jump boundary condition can be expressed as:

$$T = T_w - \frac{2-\sigma_t}{\sigma_t}\frac{2\gamma}{(\gamma+1)Pr}\sqrt{\frac{\pi\psi}{2}}\frac{\mu\ (\beta_{\mathrm{PL}})_{\mathrm{T}}}{\rho}(v.\nabla T) \tag{13}$$

4. Test case

The numerical simulation for gas flow in micro-nozzles have been carried out for different combinations of inlet pressure and back pressures as indicated in Table 2. The ratio of inlet and back pressures has been kept fixed at 10. The geometry of the micronozzle is kept constant, and the dimensions of the micro-nozzle are presented in Tab.1. Knudsen number is changed by varying the inlet and back pressures. Nitrogen (N_2) has been used as the working gas, and the associated throat Reynolds number range from 5 to 500. All the test cases have been treated as laminar. Structured meshes with linear grading have been used in all the test cases (generated using *blockMesh* utility of OpenFOAM), and

mesh convergence study has been reported in the next section.

Figure 3 shows the geometry of the simulated DSMC micronozzle with the dimensions as specified in Tab. 1. A structured grid with linear grading has been implemented, while insuring that the cell size is less than molecular MFP i.e. $(\Delta x, \Delta y) < \lambda/3$ [11]. The nitrogen gas with a molecular mass of 46.5×10^{-27} kg, viscosity index of 0.74 and the molecular diameter of 4.17×10^{-10} m is taken as the working gas. The wall and inlet temperatures are set at 300K. Wall momentum and thermal accommodation coefficients are set to unity for all the cases. The outlet and inlet pressures are varied as in the Tab. 2. A time step of 5×10^{-12} seconds is employed for all cases. A total of 20 particles per cell were simulated. The steady-state is achieved after 400000 time steps and the results are averaged for 2×10^6 time steps.

For CFD simulations, a linearly graded structured grid consisting of a total of 26400 cells has been used. The nitrogen gas with a molar mass of 28.0134×10^{-3} kg, Sutherland's coefficients : A_s and T_s as 1.41×10^{-6} kg/(s.m.K$^{1/2}$) and 111K, respectively, and Prandtl number (Pr) of 0.72 is taken as the working gas. We consider the gas to be calorically perfect for which $p = RT$ and $e = c_v T = (\gamma - 1)RT$, where R is the gas constant and $\gamma = c_p/c_v$ is the ratio of specific heats at constant pressure (c_p) and volume (c_v). The wall and inlet temperatures are set at 300K. Wall momentum and thermal accommodation coefficients are set to unity for all the cases. The outlet and inlet pressures are varied as in the Tab. 2. A time step of 5×10^{-12} seconds is employed for all cases, and the results are taken at t=1×10^{-5} seconds. Root Mean Square (RMS) of residuals were kept below 1×10^{-6}. The results of N-S-F equations with the conventional slip/jump conditions (Eqs. 7 and 8) are referred as "*Conventional slip model* ", while the results with the Knudsen layer effects are denoted as "*Knudsen layer model* ".

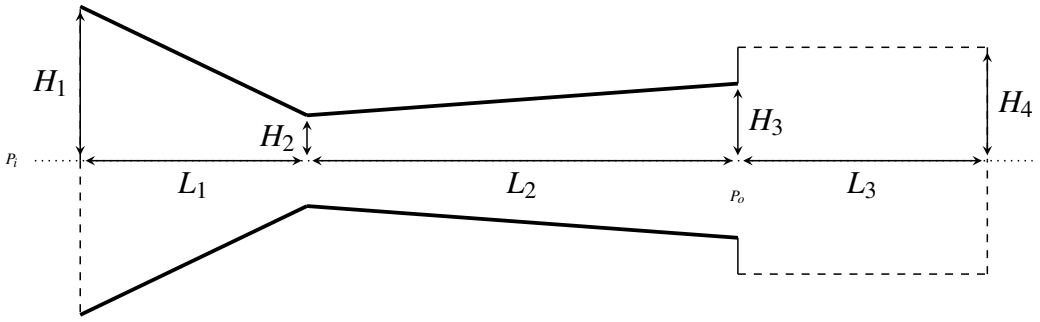

FIGURE 3: Numerical setup for micronozzle flow case [2, 10], where i, and o denote inlet, and outlet conditions respectively.

L_1	L_2	L_3	H_1	H_2	H_3	H_4
50	95	55	34	10	17	25

TABLE 1: Dimensions (in μm) of the micronozzle geometry [10]. The dimensioning labels have been defined in Fig. (3).

Case	$P_i(Pa)$	$P_o(Pa)$	Kn	$T_\infty(K)$	$n_\infty(molecules/m^3)$
1	33774	3377.4	0.0023	300	8.1558e+24
2	15768	1576.8	0.005	300	3.80e+24
3	7884.18	788.41	0.01	300	1.904e+24
4	3377.4	337.74	0.023	300	8.1558e+23
5	1576.8	157.68	0.05	300	3.80e+23

TABLE 2: Parametric variations of the test case, where ∞ denotes the free-stream condition.

4.1. Validation

Figure 3 shows the micronozzle geometry that was experimentally investigated by Hao et al. [7], and numerically investigated by Xie et al. [2] and Saadati et al. [10]. We compare the normalized pressure distribution along the centerline of computational domain i.e $Y = 0$. For the first test case of Tab. 2, Fig. 4 shows the comparison between the solutions obtained using our DSMC simulations and data reported by Saadati et al. [10]. An excellent agreement is obtained between the two solutions.

4.2. Grid Independence Study

For DSMC simulations, the computational cost depends on the total number of simulated particles, which is consecutively decided by number of cells and the number of particles per cell (PPC). There-

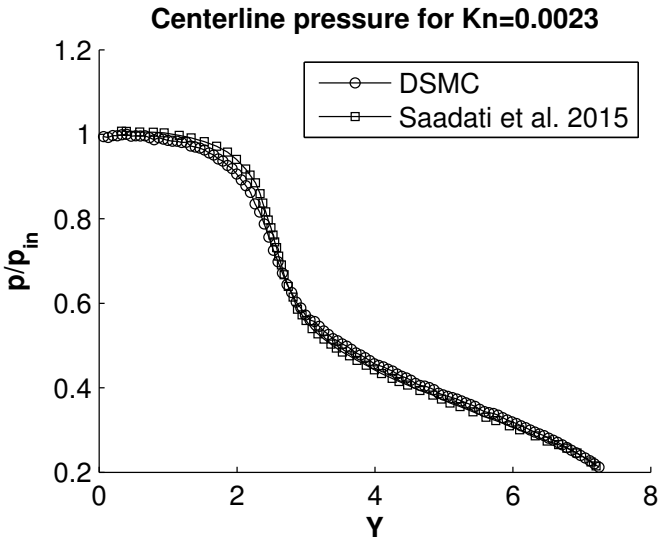

FIGURE 4: Comparison of DSMC data with the Ref. [10]

fore, a careful study of total number of cells employed is required to prevent the rise of computational cost, while also insuring that $(\Delta x, \Delta y) < \lambda/3$ [11]. With decrease in pressure and increase in MFP in axial direction, the cell-size can be increased in the micro-nozzle outlet region. Figure (5) shows the comparison between the centerline DSMC pressure distribution of micronozzle for three different grid sizes and Knudsen number of 0.0023. Based upon the results, we choose 110x40 as the final grid-size while considering the micro-nozzle symmetry i.e. only upper half of the micronozzle has been simulated to avoid unnecessary compuational cost.

To ensure that the results are independent of mesh resolution, the CFD simulations for $Kn = 0.0023$ are also carried out for three grids with different cell sizes. The grid dependency studies showed that a decrease of the cell-size in the wall normal direction is found to be necessary to obtain solutions for cases with high rarefaction levels. Figure 6 shows the comparison between the throat pressure distribution of micronozzle for three different grid sizes with cell number variation in radial and axial directions for Knudsen number of 0.0023. As per the results, the grid size of 145x120 has been selected for CFD simulations.

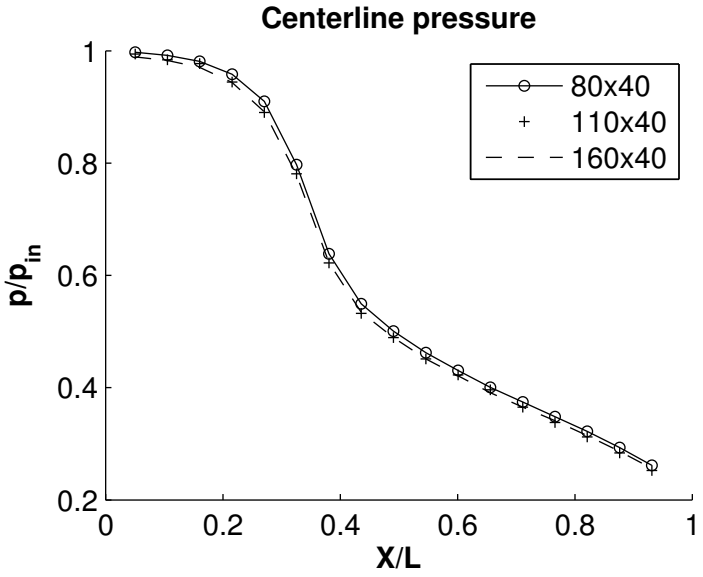

FIGURE 5: DSMC grid independence study using centerline pressure distribution as the parameter.

5. Results and Discussion

5.1. Integral Flow parameters

Figure 7 shows the centerline pressure profile for different test cases as described in Tab 2. Both the *conventional slip* and *knudsen layer* models exhibit excellent agreement for the centerline pressure distribution. The pressure at inlet, throat, and inlet compares very well for all three simulation modes i.e DSMC, CSM, KLM, and for all Knudsen numbers. However, this may not be indicative of rarefaction effects in micronozzles and hence the associated flow behaviour. A closer look at results of Mach number distribution in Fig.8, reveals that the predictions of conventional continuum model i.e. CSM deviates from the predictions of particle based DSMC simulations which increases with increase in rarefaction levels.

It is also evident from Fig. 8 that in the slip and early transition regime, nonequilibrium effects are no longer limited to the wall-adjacent layer, but prevail in the bulk flow due to the formation of Knudsen layers. So, simply using a higher-order slip model (i.e. CSM) with modified slip coefficients may result in good wall slip-velocity results but will not improve the overall predictive capabilities of the N-S-F equations into the slip regime. To improve the integral flow parameters, it is essential that

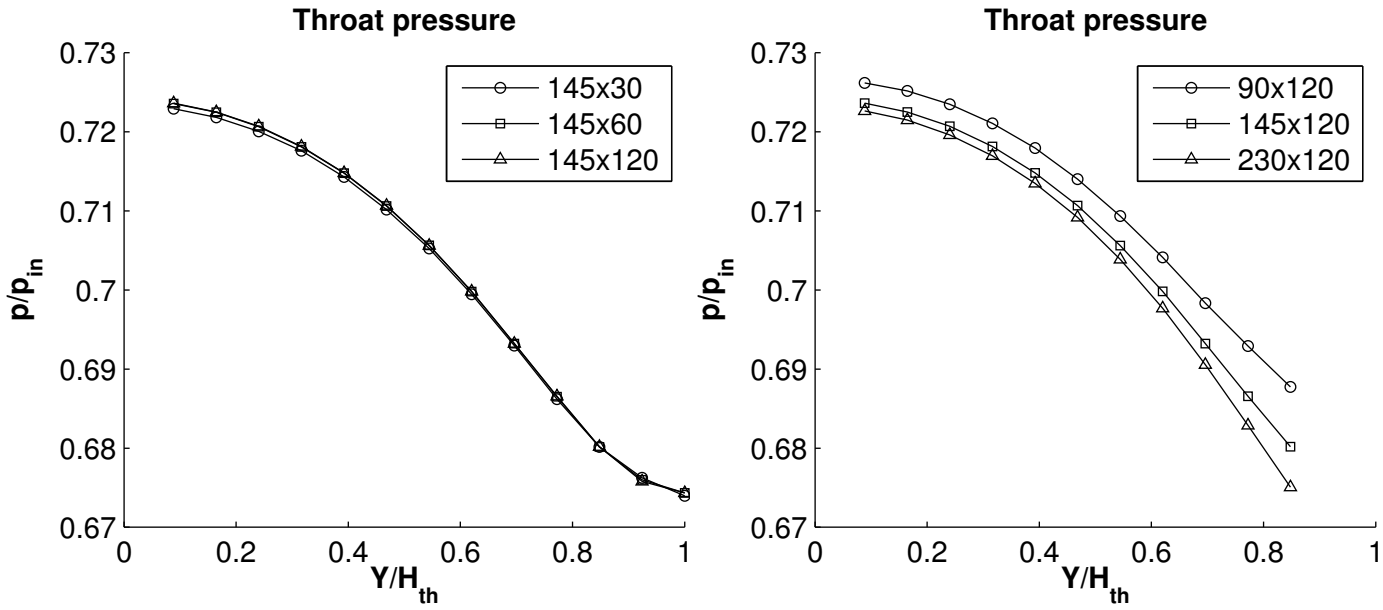

(a) (b)

FIGURE 6: N-S-F grid independence study using throat pressure as parameter in radial (Fig. 6a) and axial (Fig. 6b) directions respectively.

field variables such as MFP, viscosity and thermal conductivity are adequently accounted, which is done through our effective *Knudsen layer model* .

Figure 8 shows the centerline mach number profile for various Knudsen numbers. *Conventional slip model* significantly underpredicts the Mach number in the diverging section of the nozzle. *Knudsen layer model* shows a considerable improvement in the centerline Mach number prediction. The improvement can be also seen in the diverging part of nozzle. Near to the exit region, the *knudsen layer model* only slightly underpredicts the mach number. It is also found that the sonic conditions at throat are not achievable due to boundary layer growth. Hence, the results exihibit a subsonic flow, which is in accordance with results reported in literature [9, 10]. Figures 8 and 12 also depicts two particular phenomena in the micronozzle flow. The first one is the position of sonic point that moves away from the throat to the outlet of the micro nozzle with the increase in Knudsen number. While the second one is the outlet Mach number that decreases for higher rarefaction levels.

The throat velocity profiles for different Knudsen numbers are presented in Fig. 9. As stated previ-

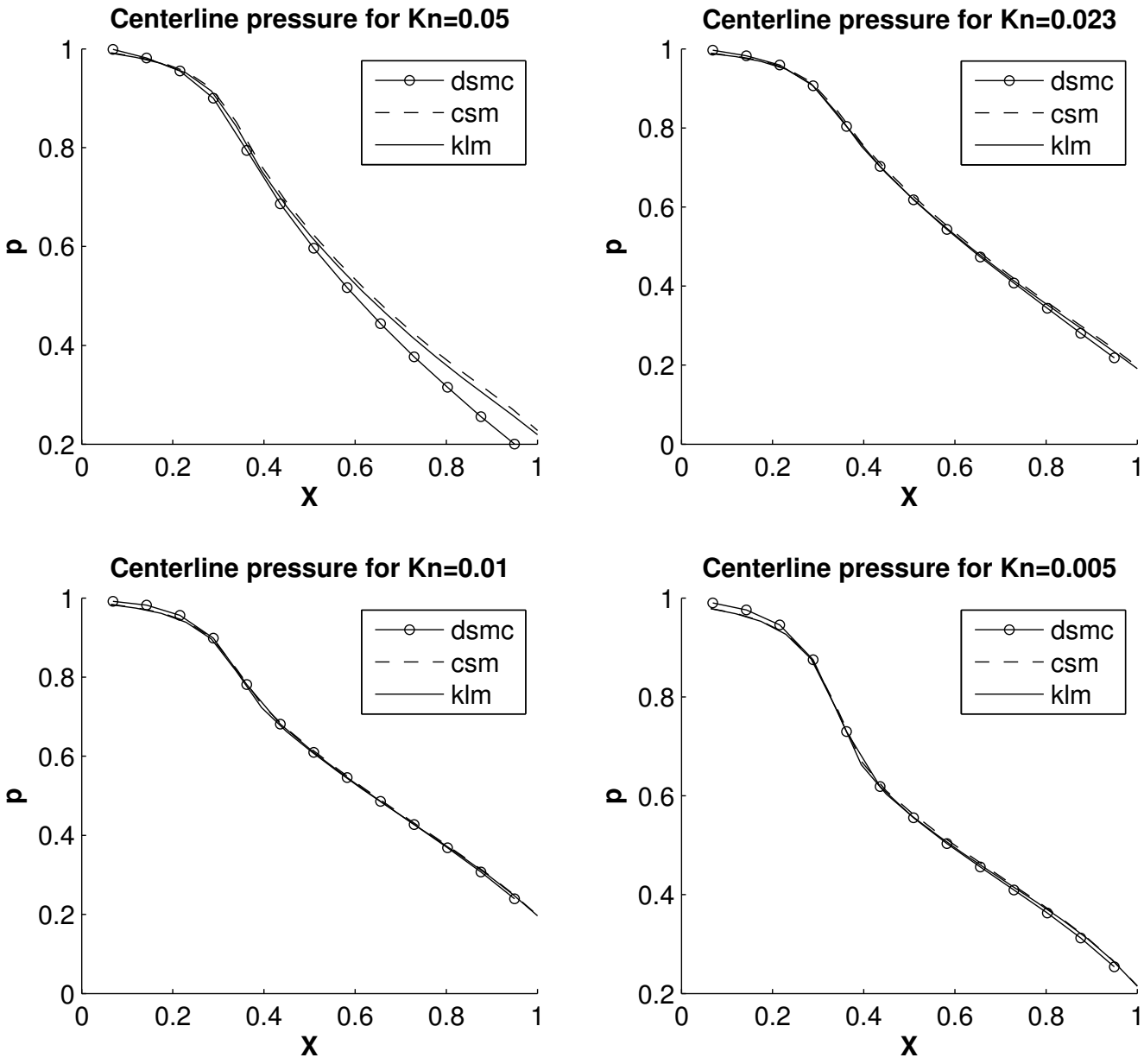

FIGURE 7: Variation of centerline pressure for different Knudsen numbers.

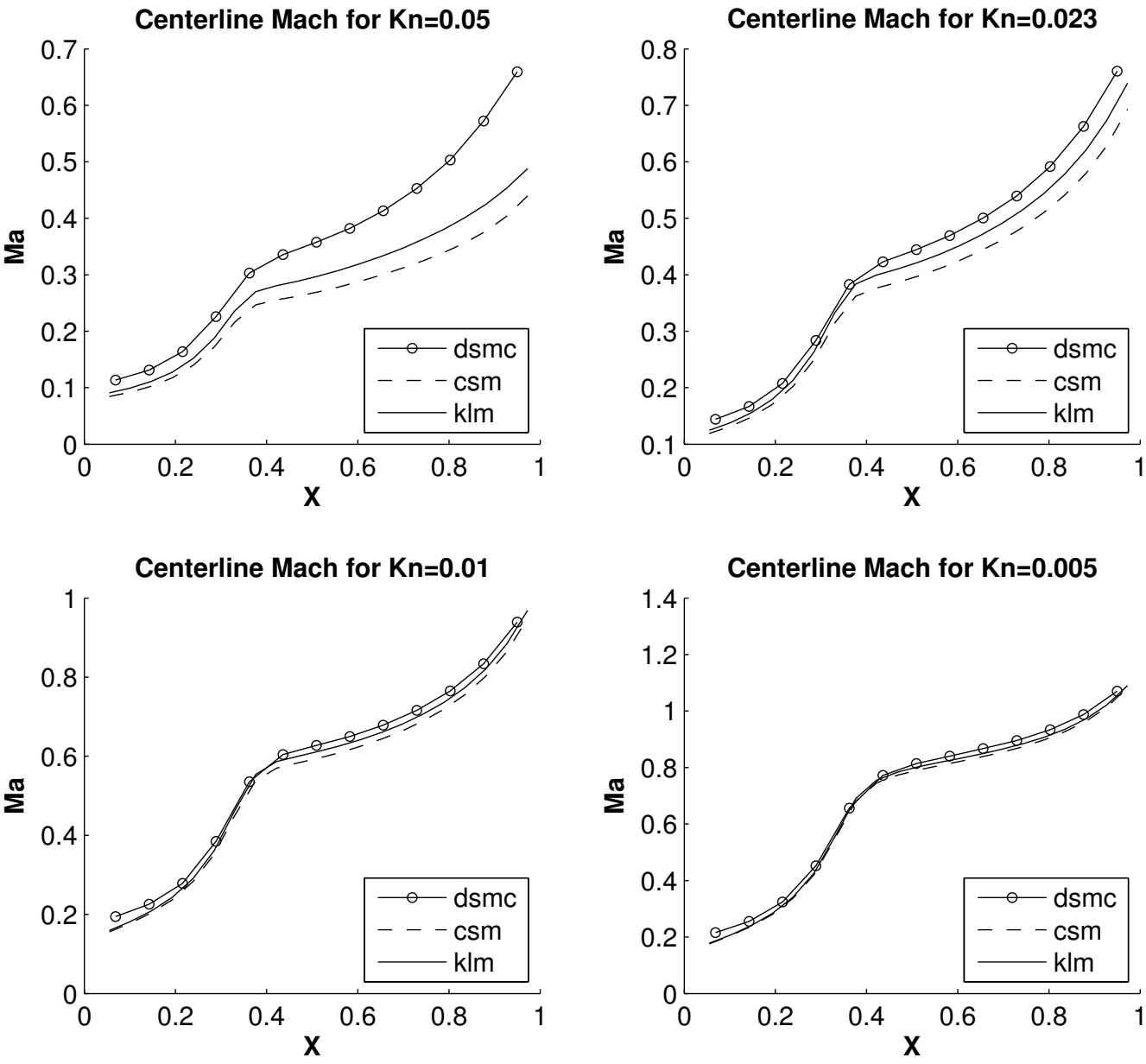

FIGURE 8: Variation of centerline mach number for different Knudsen numbers.

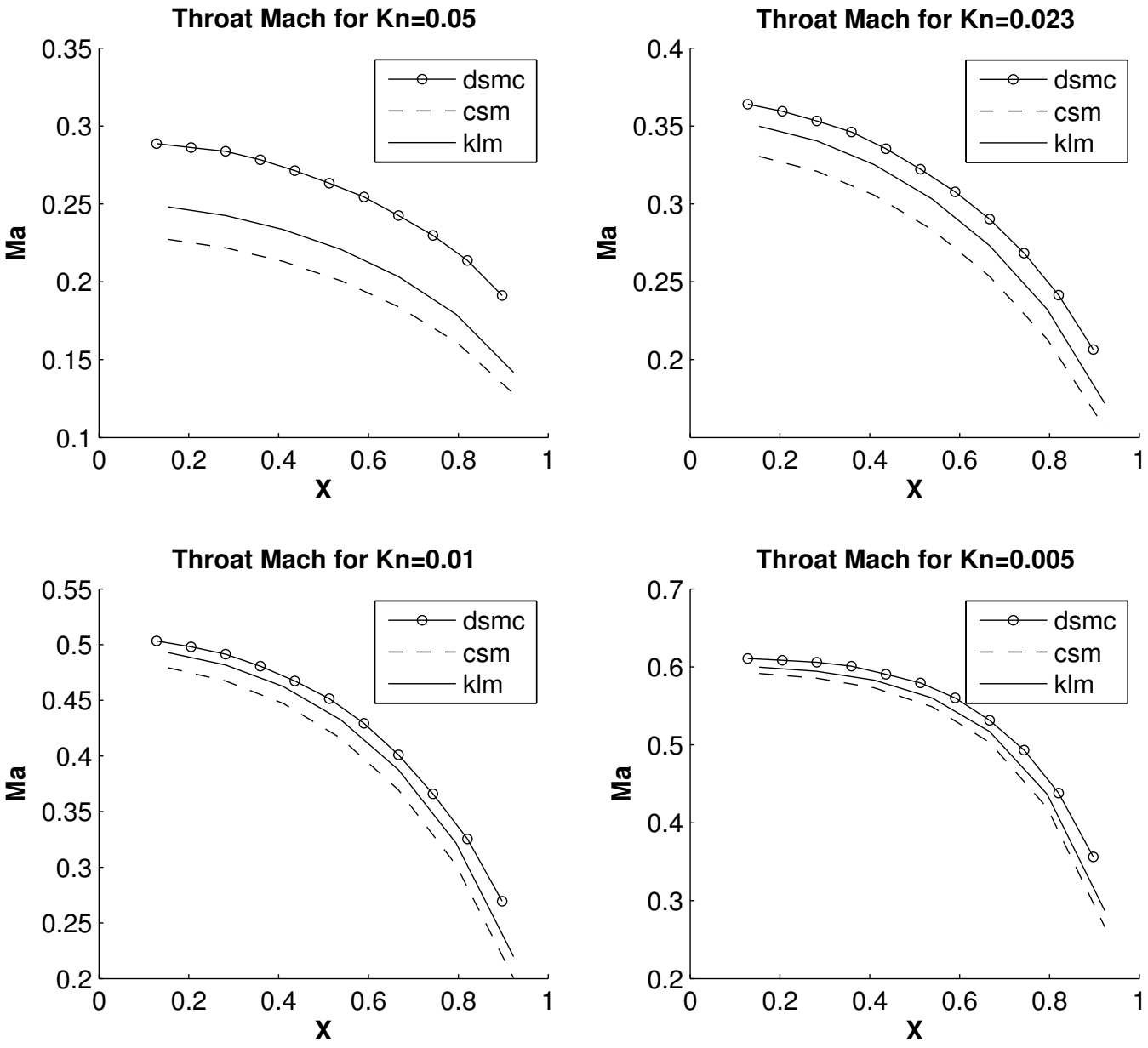

FIGURE 9: Variation of throat mach number for different Knudsen numbers.

ously, the flow measurements at *selected points* of micro-nozzle might not be indicative of the dynamics of the entire flow. The radial variations in Mach number at throat embraces the same. A significant deviation between conventional N-S-F and DSMC results is observed at even lower Knudsen numbers. Our *Knudsen layer model* considerably improves the predictions of flow properties and reduces the difference between conventional N-S-F equations and DSMC predictions by approximately 50%. Incorporation of higher order constitutive relations such as Burnett equations [9, 51], grad-moment equation models such as R26 [16, 17], and second-order Kinetic Boltzmann equations [52] in our model can further narrow down the difference between DSMC and *Knudsen layer model* predictions.

5.2. The Subsonic Viscous Layer

In the near wall region, especially at low *Re*, the viscous diffusion plays a dominant role in determing the flow characteristics in the micro-nozzle. Owing to the inherently low Reynolds number, substantial viscous subsonic layers develop on the walls of the micro-nozzle. The thickness of viscous subsonic layer away from the wall (Knudsen Layer) in the bulk region of micro-nozzle is governed by associated rarefaction level i.e high Knudsen numbers. Higher degrees of rarefaction results in a lower mass through the micro/nano nozzle. The viscous subsonic layer retards the bulk flow, and reduces the nozzle performance.

The viscous subsonic layer throughout the micronozzle has been illustrated in Fig. 12. Only the portion of the flow configuration where Mach number is below unity, has been depicted in these figures. These profiles provide a comparative measure of the strength of viscous forces and the influence of the Knudsen layer on the flow field. It is observed that a higher Knudsen number results in a smaller average Mach number at the nozzle throat, owing to the increased thickness of viscous layer. The thickness of viscous layer at the nozzle exit, expressed as a percentage of the nozzle exit dimensions, has been depicted in Fig. 10. It can be inferred that the thickness of viscous layer scales inversly with Reynolds number, and proportionately (non-linear relation) with Knudsen number. Moreover, the subsonic viscous layer fills the entire domain even at *Kn* as low as 0.05.

The specific impulse (i.e., thrust per unit mass) is an important design and flow parameter of interest

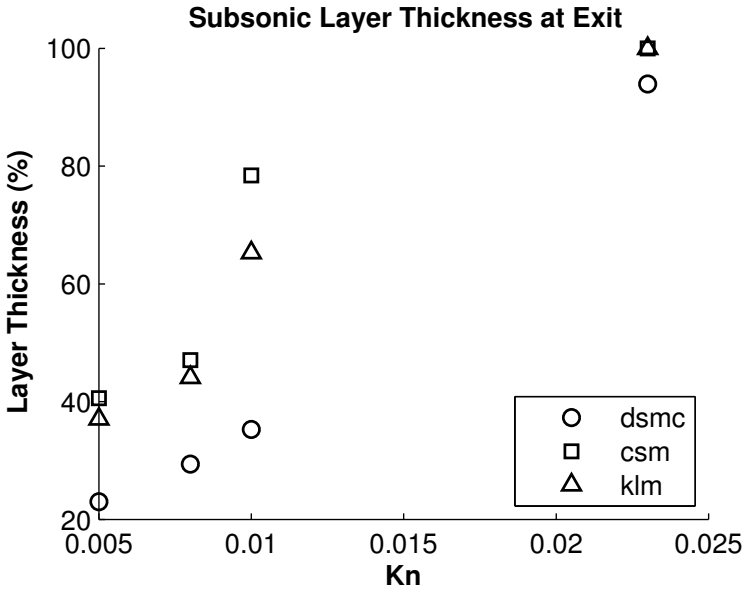

FIGURE 10: The thickness of viscous subsonic layers at the micronozzle exit plane depicted as a function of Knudsen number.

which is indicative of the performance of micronozzles. Theoretically, it gives a quantitative measure of total impulse delivered per unit of propellant consumed. An under-prediction of I_{sp} value can lead to over design of micronozzle. At the nozzle exit, the thrust per unit mass has been delineated as a function of Knudsen number in Fig. 11. The I_{sp} predictions from conventional N-S-F equations are significantly lower than the DSMC predictions. At lower Knudsen numbers, the results of *Knudsen layer model* are in accordance with the DSMC predictions. At $Kn = 0.023$, our model shows an improvement in predictions by $\sim 50\%$. It is observed that the magnitude of specific impulse decreases with increase in Knudsen number, and the relation between the two variables is non-linear which is attributed to the presence of thicker subsonic layers at high Knudsen numbers, that inherently retards the bulk flow and thus reduces the thrust generated.

5.3. Wall-Shear Stress

The presence of thick viscous layers affects the "wall shear stress" considerably. Figure 13 shows the wall shear stress for $Kn = 0.05$. The rarefaction effects are not captured by the *conventional slip model* . The results from *knudsen layer model* and *conventional slip model* shows a substantial difference of 50% to 80% in shear stress predictions at various cross sections of the micronozzle. This

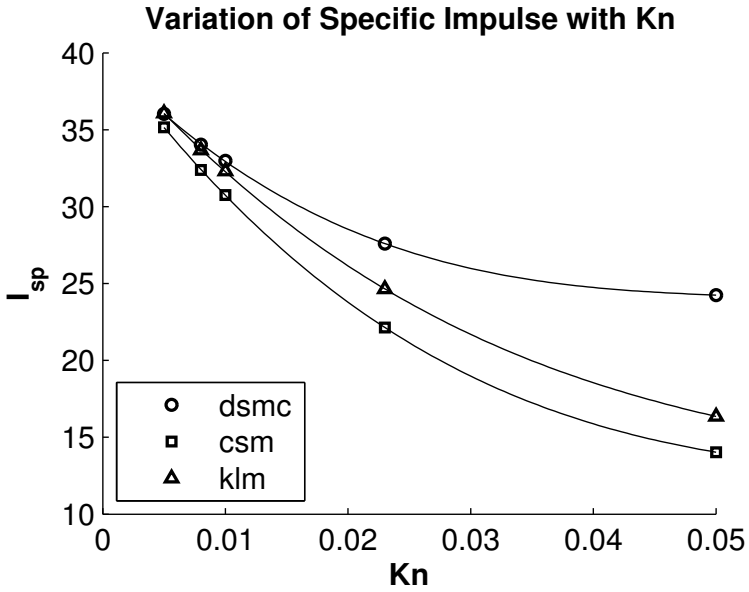

FIGURE 11: The specific impulse at the micronozzle exit plane delineated as a function of Knudsen number with different simulation modes. The curve shown above, has been obtained using third order polynomial curve fitting of given data points.

difference gets more pronounced at higher Knudsen numbers.

Mach number and local Knudsen number are two parameters that affect the shear stress at walls. In the converging portion of micronozzle, both the parameters increase very rapidly and so does the wall-shear stress. As soon as the flow enters the diverging portion of micronozzle, the ***rate of increase*** in Mach number and local Knudsen number decreases. And, hence a rapid decrease in shear stress value is observed in immediate vicinity of the throat. However as the flow stablizes afterwards, the ***rate of decrease*** in shear-stress decreases.

6. Conclusions

The expansion of nitrogen gas through a linear converging-diverging (C/D) type micronozzle at Knudsen number ranging between 0.005 and 0.05, and with Reynolds number in the range between 5 and 500, has been studied numerically using the particle and continuum methods. Various micro-nozzle configurations have been examined in order to delineate micronozzle performance characteristics, and comparisons made for specific impulse, viscous subsonic layer thickness, and wall shear stress results.

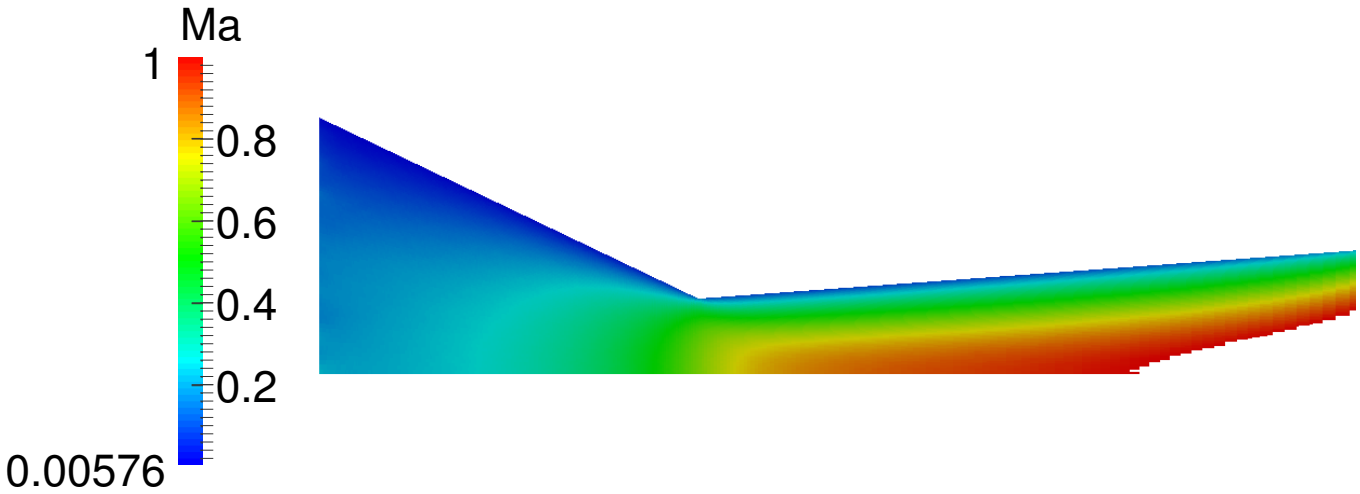

(a) $Kn = 0.005$

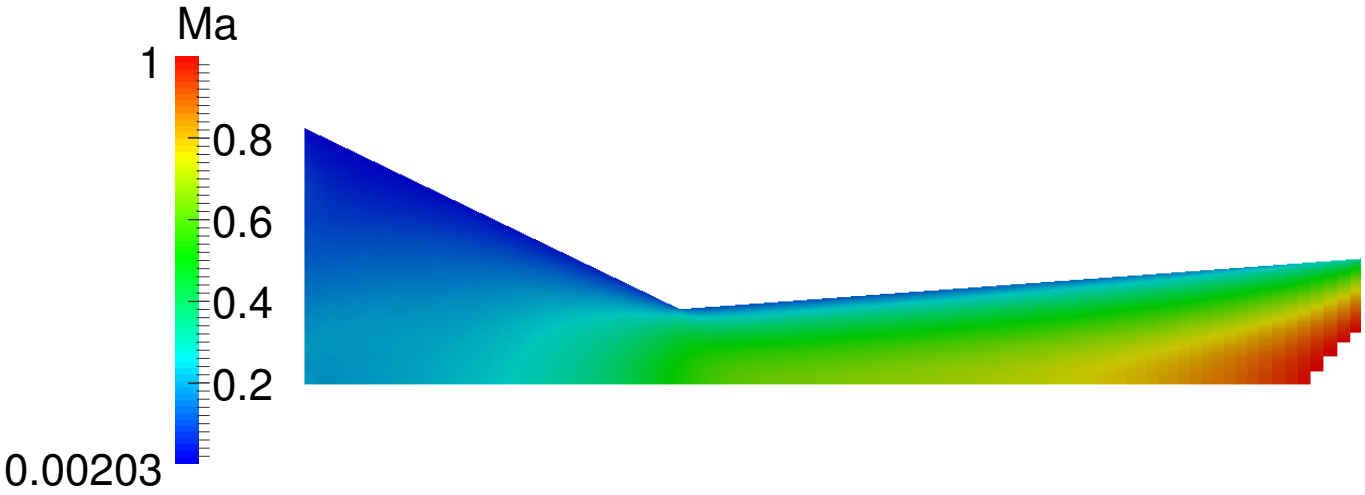

(b) $Kn = 0.01$

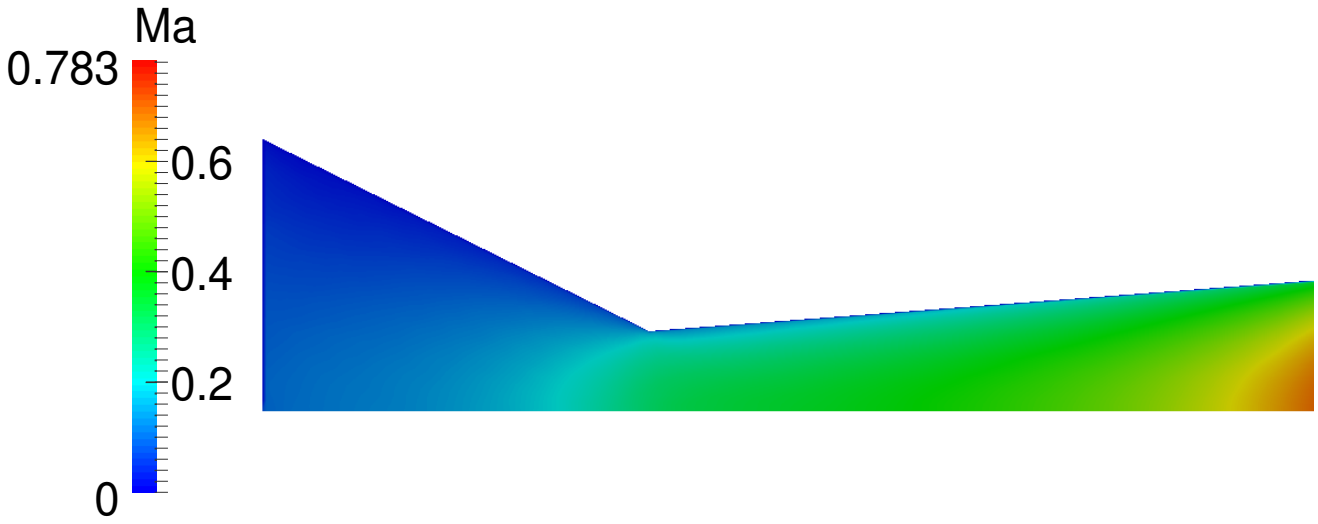

(c) $Kn = 0.05$

FIGURE 12: The contour of subsonic layers in the micronozzle at various Knudsen numbers obtained using DSMC simulations. The mesh cells have been rendered in the above figures.

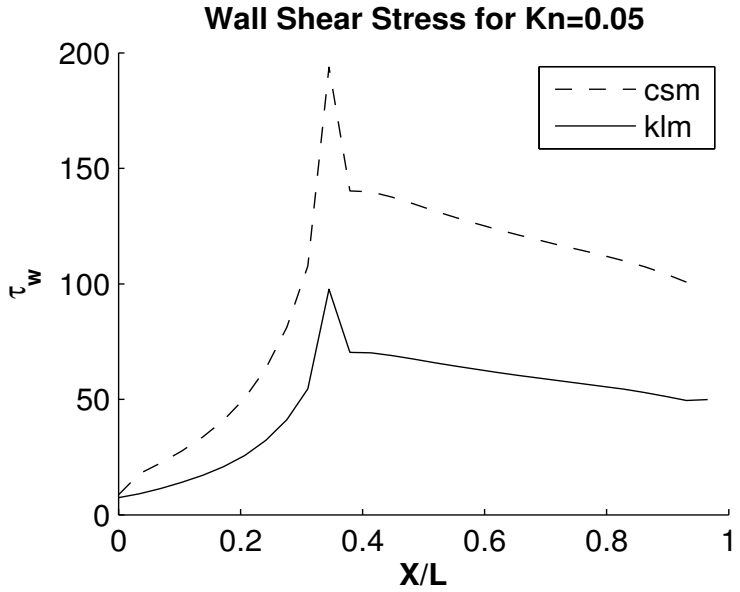

FIGURE 13: Wall Shear Stress for highest Knudsen number $Kn = 0.05$. Here, τ_w denotes the wall shear stress.

The conventional N-S-F model overpredicts specific impulse which inherently adds dead-weight to the system and further leads to nozzle over-design. KLM model improves these predictions by as much as 50% when compared to conventional N-S-F results.

Analysis of the micronozzle flowfield has shown that the subsonic layers from opposing nozzle walls can grow sufficiently large and merge together in the nozzle expander section for linear C/D geometries. The consequence of this merging is that the entire cross section of the flowfield at the nozzle exit plane is completely subsonic, and as such the specific impulse is severely degraded. This finding is in agreement with Ref. [53], where an inverse dependence of performance with viscous-layer thickness has been reported.

DSMC and KLM methodologies capture many of the trends associated with the complex non-equilibrium physics of the rarefied gas flows. With the incorporation of Knudsen-layer effects, we can improve the predictive capabilities of the N-S-F framework for simulating rarefied supersonic pressure-driven micronozzle gas flows. The future importance of this paper stems from the fact that the Knudsen layer implementation is carried out in an open-source CFD software and indeed with the additional

computational cost to be negligible. The tool can be run in parallel, and therefore can be applied to test complex geometries involving unstructured grids.

Acknowledgments

The research leading to these results has received funding from the Department of Science and Technology (DST) India under the INSPIRE Faculty Award. The author VKS would like to thank Department of Atomic Energy (DAE) India for support through Homi Bhabha Chair at IIT Hyderabad.

References

[1] HO, C.-M., AND TAI, Y.-C. Micro-electro-mechanical-systems (mems) and fluid flows. *Annual Review of Fluid Mechanics 30*, 1 (1998), 579–612.

[2] XIE, C. Characteristics of micronozzle gas flows. *Physics of Fluids (1994-present) 19*, 3 (2007), 037102.

[3] SONE, Y. *Kinetic theory and fluid dynamics*. Springer Science & Business Media, 2002.

[4] MILLIGAN, M. W. Nozzle characteristics in the transition regime between continuum and free molecular flow. *AIAA Journal 2*, 6 (1964), 1088–1092.

[5] ROTHE, D. E. Electron-beam studies of viscous flow in supersonic nozzles. *AIAA Journal 9*, 5 (1971), 804–811.

[6] BOYD, I. D., PENKO, P. F., MEISSNER, D. L., AND DEWITT, K. J. Experimental and numerical investigations of low-density nozzle and plume flows of nitrogen. *AIAA journal 30*, 10 (1992), 2453–2461.

[7] HAO, P.-F., DING, Y.-T., YAO, Z.-H., HE, F., AND ZHU, K.-Q. Size effect on gas flow in micro nozzles. *Journal of Micromechanics and Microengineering 15*, 11 (2005), 2069.

[8] XU, J., AND ZHAO, C. Two-dimensional numerical simulations of shock waves in micro convergent–divergent nozzles. *International Journal of Heat and Mass Transfer 50*, 11 (2007), 2434–2438.

[9] SAN, O., BAYRAKTAR, I., AND BAYRAKTAR, T. Size and expansion ratio analysis of micro nozzle gas flow. *International Communications in Heat and Mass Transfer 36*, 5 (2009), 402–411.

[10] SAADATI, S. A., AND ROOHI, E. Detailed investigation of flow and thermal field in micro/nano nozzles using simplified bernoulli trial (sbt) collision scheme in dsmc. *Aerospace Science and Technology 46* (2015), 236–255.

[11] BIRD, G. A. Molecular gas dynamics and the direct simulation of gas flows.

[12] SCANLON, T., ROOHI, E., WHITE, C., DARBANDI, M., AND REESE, J. An open source, parallel dsmc code for rarefied gas flows in arbitrary geometries. *Computers & Fluids 39*, 10 (2010), 2078–2089.

[13] ORAN, E., OH, C., AND CYBYK, B. Direct simulation monte carlo: recent advances and applications 1. *Annual Review of Fluid Mechanics 30*, 1 (1998), 403–441.

[14] KARNIADAKIS, G., BESKOK, A., AND ALURU, N. *Microflows and nanoflows: fundamentals and simulation*, vol. 29. Springer Science & Business Media, 2006.

[15] CERCIGNANI, C. *The Boltzmann equation*. Springer, 1988.

[16] CHEN, S., AND DOOLEN, G. D. Lattice boltzmann method for fluid flows. *Annual review of fluid mechanics 30*, 1 (1998), 329–364.

[17] ANSUMALI, S., KARLIN, I., ARCIDIACONO, S., ABBAS, A., AND PRASIANAKIS, N. Hydrodynamics beyond navier-stokes: Exact solution to the lattice boltzmann hierarchy. *Physical review letters 98*, 12 (2007), 124502.

[18] GUO, Z., SHI, B., AND ZHENG, C. G. An extended navier-stokes formulation for gas flows in the knudsen layer near a wall. *Europhysics Letters 80*, 2 (2007), 24001.

[19] STOPS, D. The mean free path of gas molecules in the transition regime. *Journal of Physics D: Applied Physics 3*, 5 (1970), 685.

[20] LOCKERBY, D. A., AND REESE, J. M. On the modelling of isothermal gas flows at the microscale. *Journal of Fluid Mechanics 604* (2008), 235–261.

[21] DONGARI, N., ZHANG, Y., AND REESE, J. M. Molecular free path distribution in rarefied gases. *Journal of Physics D: Applied Physics 44*, 12 (2011), 125502.

[22] ARLEMARK, E. J., DADZIE, S. K., AND REESE, J. M. An extension to the navier–stokes equations to incorporate gas molecular collisions with boundaries. *Journal of Heat Transfer 132*, 4 (2010), 041006.

[23] DONGARI, N., ZHANG, Y., AND REESE, J. M. Modeling of knudsen layer effects in micro/nanoscale gas flows. *Journal of Fluids Engineering 133*, 7 (2011), 071101.

[24] GUO, Z., QIN, J., AND ZHENG, C. Generalized second-order slip boundary condition for nonequilibrium gas flows. *Physical Review E 89*, 1 (2014), 013021.

[25] NOROUZI, A., AND ESFAHANI, J. A. Two relaxation time lattice boltzmann equation for high knudsen number flows using wall function approach. *Microfluidics and Nanofluidics 18*, 2 (2015), 323–332.

[26] DONGARI, N. *Micro Gas Flows: Modelling the Dynamics of Knudsen Layers*. Phd thesis, University of Strathclyde, Glasgow, U.K, 2012.

[27] DONGARI, N., BARBER, R. W., EMERSON, D. R., STEFANOV, S. K., ZHANG, Y., AND REESE, J. M. The effect of knudsen layers on rarefied cylindrical couette gas flows. *Microfluidics and nanofluidics 14*, 1-2 (2013), 31–43.

[28] DONGARI, N., WHITE, C., SCANLON, T. J., ZHANG, Y., AND REESE, J. M. Effects of curvature on rarefied gas flows between rotating concentric cylinders. *Physics of Fluids (1994-present) 25*, 5 (2013), 052003.

[29] ZHANG, Y.-H., GU, X.-J., BARBER, R. W., AND EMERSON, D. R. Capturing knudsen layer phenomena using a lattice boltzmann model. *Physical Review E 74*, 4 (2006), 046704.

[30] JAISWAL, S., AND DONGARI, N. Implementation of knudsen layer effects in open source cfd solver for effective modeling of microscale gas flows. In *Proceedings of 23rd National and 1st International ISHMT-ASTFE Heat and Mass Transfer conference* (December 2015), ISHMT-ASTFE. Paper No: IHMTC2015-1450.

[31] WHITE, C. *Benchmarking, Development and Applications of an Open Source DSMC Solver*. Phd thesis, University of Strathclyde, Glasgow, U.K, May 2013.

[32] GREENSHIELDS, C. J., WELLER, H. G., GASPARINI, L., AND REESE, J. M. Implementation of semi-discrete, non-staggered central schemes in a colocated, polyhedral, finite volume framework, for high-speed viscous flows. *International journal for numerical methods in fluids 63*, 1 (2010), 1–21.

[33] WELLER, H. G., TABOR, G., JASAK, H., AND FUREBY, C. A tensorial approach to computational continuum mechanics using object-oriented techniques. *Computers in physics 12*, 6 (1998), 620–631.

[34] JASAK, H., JEMCOV, A., AND TUKOVIC, Z. Openfoam: A c++ library for complex physics simulations.

[35] STROUSTRUP, B. *The C++ programming language*. Pearson Education India, 1986.

[36] KURGANOV, A., AND TADMOR, E. New high-resolution central schemes for nonlinear conservation laws and convection–diffusion equations. *Journal of Computational Physics 160*, 1 (2000), 241–282.

[37] KURGANOV, A., NOELLE, S., AND PETROVA, G. Semidiscrete central-upwind schemes for hyperbolic conservation laws and hamilton–jacobi equations. *SIAM Journal on Scientific Computing 23*, 3 (2001), 707–740.

[38] GREENSHIELDS, C. J., AND REESE, J. M. Rarefied hypersonic flow simulations using the navier–stokes equations with non-equilibrium boundary conditions. *Progress in Aerospace Sciences 52* (2012), 80–87.

[39] BOHORQUEZ, P., AND PARRAS, L. Three-dimensional numerical simulation of the wake flow of an afterbody at subsonic speeds. *Theoretical and Computational Fluid Dynamics 27*, 1-2 (2013), 201–218.

[40] MOHAMMADZADEH, A., ROOHI, E., NIAZMAND, H., STEFANOV, S., AND MYONG, R. S. Thermal and second-law analysis of a micro-or nanocavity using direct-simulation monte carlo. *Physical Review E 85*, 5 (2012), 056310.

[41] LE, N. T., WHITE, C., REESE, J. M., AND MYONG, R. S. Langmuir–maxwell and langmuir–smoluchowski boundary conditions for thermal gas flow simulations in hypersonic aerodynamics. *International Journal of Heat and Mass Transfer 55*, 19 (2012), 5032–5043.

[42] LIOU, W., AND FANG, Y. Implicit boundary conditions for direct simulation monte carlo method in mems flow predictions. *CMES- Computer Modeling in Engineering & Sciences 1*, 4 (2000), 119–128.

[43] FANG, Y., AND LIOU, W. W. Computations of the flow and heat transfer in microdevices using dsmc with implicit boundary conditions. *Journal of Heat Transfer 124*, 2 (2002), 338–345.

[44] WHITE, C., BORG, M. K., SCANLON, T. J., AND REESE, J. M. A dsmc investigation of gas flows in micro-channels with bends. *Computers & Fluids 71* (2013), 261–271.

[45] CERCIGNANI, C., FRANGI, A., LORENZANI, S., AND VIGNA, B. Bem approaches and simplified kinetic models for the analysis of damping in deformable mems. *Engineering analysis with boundary elements 31*, 5 (2007), 451–457.

[46] LOCKERBY, D. A., REESE, J. M., AND GALLIS, M. A. Capturing the knudsen layer in continuum-fluid models of nonequilibrium gas flows. *AIAA journal 43*, 6 (2005), 1391–1393.

[47] FICHMAN, M., AND HETSRONI, G. Viscosity and slip velocity in gas flow in microchannels. *Physics of Fluids (1994-present) 17*, 12 (2005), 123102.

[48] BAHUKUDUMBI, P. A unified engineering model for steady and quasi-steady shear-driven gas microflows. *Microscale Thermophysical Engineering 7*, 4 (2003), 291–315.

[49] BIRD, R. B. Transport phenomena. *Applied Mechanics Reviews 55*, 1 (2002), R1–R4.

[50] LE, N., GREENSHIELDS, C. J., AND REESE, J. Evaluation of nonequilibrium boundary conditions for hypersonic rarefied gas flows. In *Progress in Flight Physics* (2012), vol. 3, EDP Sciences, pp. 217–230.

[51] AGARWAL, R. K., YUN, K.-Y., AND BALAKRISHNAN, R. Beyond navier–stokes: Burnett equations for flows in the continuum–transition regime. *Physics of Fluids (1994-present) 13*, 10 (2001), 3061–3085.

[52] MYONG, R. S. Theoretical description of the gaseous knudsen layer in couette flow based on the second-order constitutive and slip-jump models. *Physics of Fluids 28*, 1 (2016).

[53] LOUISOS, W. F., AND HITT, D. L. Numerical studies of supersonic flow in bell-shaped micronozzles. *Journal of Spacecraft and Rockets 51*, 2 (2014), 491–500.